




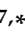



## Article

# Facile Synthesis of Low-Cost Copper-Silver and Cobalt-Silver Alloy Nanoparticles on Reduced Graphene Oxide as Efficient Electrocatalysts for Oxygen Reduction Reaction in Alkaline Media

Jadranka Milikić<sup>1,\*</sup>, Sara Knežević<sup>2</sup>, Stevan Stojadinović<sup>3</sup>, Mabkhoot Alsaiari<sup>4,5</sup>, Farid A. Harraz<sup>4,6</sup>, Diogo M. F. Santos<sup>7,\*</sup> and Biljana Šljukić<sup>1,7</sup>

<sup>1</sup> University of Belgrade, Faculty of Physical Chemistry, Studentski trg 12-16, 11158 Belgrade, Serbia; biljka@ffh.bg.ac.rs

<sup>2</sup> Faculty of Chemistry, University of Belgrade, Studentski trg 12-16, 11000 Belgrade, Serbia; packdatc@gmail.com

<sup>3</sup> University of Belgrade, Faculty of Physics, Studentski trg 12-16, 11000 Belgrade, Serbia; sstevan@ff.bg.ac.rs

<sup>4</sup> Promising Centre for Sensors and Electronic Devices (PCSED), Advanced Materials and Nano-Research Centre, Najran University, Najran 11001, Saudi Arabia; mamalsaiari@nu.edu.sa (M.A.); faharraz@nu.edu.sa (F.A.H.)

<sup>5</sup> Department of Chemistry, Faculty of Science and Arts at Sharurah, Najran University, Najran 11001, Saudi Arabia

<sup>6</sup> Nanomaterials and Nanotechnology Department, Central Metallurgical Research and Development Institute (CMRDI), Helwan 11421, Cairo, Egypt

<sup>7</sup> Center of Physics and Engineering of Advanced Materials, Laboratory for Physics of Materials and Emerging Technologies, Chemical Engineering Department, Instituto Superior Técnico, Universidade de Lisboa, 1049-001 Lisbon, Portugal

\* Correspondence: jadranka@ffh.bg.ac.rs (J.M.); diogosantos@tecnico.ulisboa.pt (D.M.F.S.)



**Citation:** Milikić, J.; Knežević, S.; Stojadinović, S.; Alsaiari, M.; Harraz, F.A.; Santos, D.M.F.; Šljukić, B. Facile Synthesis of Low-Cost Copper-Silver and Cobalt-Silver Alloy Nanoparticles on Reduced Graphene Oxide as Efficient Electrocatalysts for Oxygen Reduction Reaction in Alkaline Media. *Nanomaterials* **2022**, *12*, 2657. <https://doi.org/10.3390/nano12152657>

Academic Editor: Gengtao Fu

Received: 6 July 2022

Accepted: 28 July 2022

Published: 2 August 2022

**Publisher's Note:** MDPI stays neutral with regard to jurisdictional claims in published maps and institutional affiliations.



**Copyright:** © 2022 by the authors. Licensee MDPI, Basel, Switzerland. This article is an open access article distributed under the terms and conditions of the Creative Commons Attribution (CC BY) license (<https://creativecommons.org/licenses/by/4.0/>).

**Abstract:** Copper-silver and cobalt-silver alloy nanoparticles deposited on reduced graphene oxide (CuAg/rGO and CoAg/rGO) were synthesized and examined as electrocatalysts for oxygen reduction reaction (ORR) and hydrogen peroxide reduction reaction (HPRR) in alkaline media. Characterization of the prepared samples was done by transmission electron microscopy (TEM), Fourier-transform infrared spectroscopy (FTIR), Raman spectroscopy, X-ray diffraction analysis (XRD), and scanning electron microscopy with integrated energy-dispersive X-ray spectroscopy (SEM-EDS). CuAg/rGO and CoAg/rGO nanoparticles diameter ranged from 0.4 to 9.2 nm. The Ag loading was ca. 40 wt.% for both electrocatalysts, with that for Cu and Co being 35 and 17 wt.%, respectively. CoAg/rGO electrocatalyst showed a Tafel slope of 109 mV dec<sup>-1</sup>, significantly lower than that for CuAg/rGO (184 mV dec<sup>-1</sup>), suggesting faster ORR kinetics. Additionally, a higher diffusion current density was obtained for CoAg/rGO (−2.63 mA cm<sup>-2</sup>) than for CuAg/rGO (−1.74 mA cm<sup>-2</sup>). The average value of the number of electrons transferred during ORR was 2.8 for CuAg/rGO and 3.3 for CoAg/rGO electrocatalyst, further confirming the higher ORR activity of the latter. On the other hand, CuAg/rGO showed higher peak current densities (−3.96 mA cm<sup>-2</sup>) for HPRR compared to those recorded for CoAg/rGO electrocatalyst (−1.96 mA cm<sup>-2</sup>).

**Keywords:** oxygen reduction reaction; hydrogen peroxide reduction reaction; nanoparticles; CuAg alloy; CoAg alloy; reduced graphene oxide

## 1. Introduction

As the energy demand increases over the years, the amount of available fossil fuels decreases. Furthermore, the carbon emissions and other negative environmental impacts of using fossil fuels deepen the need for clean energy sources. That is why electrochemical energy conversion and storage devices like fuel cells and batteries, which are green, renewable, and have high energy density output, are essential.

Both oxygen reduction reaction (ORR) and hydrogen peroxide reduction reaction (HPRR) are common cathodic half-reactions in fuel cells. ORR can proceed via either a two-electron or a four-electron pathway, depending on the type of electrocatalyst and electrolyte composition. The former is more sluggish, as it takes place in two steps—hydrogen peroxide formation and the hydrogen peroxide reduction reaction (HPRR), whereas the latter, the one-step process, is favored [1–3].

Regardless of the reaction pathway, energy investment is essential for diffusion, adsorption, desorption, bond breakage, and bond formation to occur and transform  $O_2$  into the reaction products ( $OH^-$  or  $H_2O$ ). Furthermore, the need to break the high-energy  $O=O$  bond increases the energy barrier, making this reaction at least ten times slower than HER, which is simultaneously occurring at the cathode. Consequently, it requires high overpotentials and cannot proceed without an electrocatalyst [4].

Since  $H_2O_2$  is a reaction intermediate in ORR, it can (under certain conditions) be the final product of a two-electron reduction process [5–7]. Ideally, the catalysts for ORR should be active for the HPRR. Furthermore, although oxygen is an available and affordable reactant, HPRR has certain advantages over ORR. Namely, as a two-electron process with faster kinetics and higher electrode potential, it results in a higher voltage of the system. Utilizing liquid reactants instead of gaseous ones facilitates handling, storage, and transport and eliminates the need for complicated fuel cell construction and gas management [2]. Thus, HPRR-based fuel cells can have lower activation energy and better stability, ease of handling, and storage than those based on ORR [8]. HPRR can proceed by a direct mechanism, involving a two-electron reduction to water, which is preferred, or by an indirect mechanism that involves  $H_2O_2$  decomposition to  $O_2$  and its subsequent reduction [1].

Generally, platinum group metal (PGM)-based catalysts were used for ORR due to their ability to decrease the activation energy and the required critical oxygen concentration. Still, high cost, an easy poisoning limit, and scarcity limit their applicability [9,10]. Consequently, many transition metals [11–13], metal oxides [14–16], metal-organic frameworks (MOFs) [17,18], zeolitic imidazolate frameworks (ZIFs) [17,18], and carbon-based [19–21] catalysts have emerged as efficient and robust low-cost alternatives to PGM. Concerning HPRR, the most potent catalysts can be divided into three categories—enzymes, noble metals (PGM and Ag), and macrocycle complexes of transition metals. However, the downsides of the first and the last are their low chemical, physical, or thermal stability, and the noble metals' high price and the catalysis of  $H_2O_2$  decomposition decrease their applicability [22]. The need for low-cost, stable, biocompatible materials with high catalytic activity for HPRR has resulted in the production of transition metal oxide-based materials [8,22–24] and carbon materials [25–27].

In this work, CuAg and CoAg-doped reduced graphene oxide (rGO) are proposed as efficient electrocatalysts for ORR and HPRR in alkaline media. Alkaline media, as a less corrosive environment compared to acidic media, allows using non-noble metal catalysts for ORR [28,29]. Additionally, ORR kinetics in alkaline media have been reported to be faster than in acidic media [30,31]. Thus, ORR can proceed at lower overpotentials in alkaline media (e.g., NaOH, KOH) than in several acidic media (e.g.,  $H_2SO_4$ ,  $H_3PO_4$ ,  $HClO_4$ ). The superior performance of Pt electrocatalysts in alkaline media (KOH) than in acidic media (e.g.,  $H_3PO_4$ ) was attributed to the minimal adsorption of the  $OH^-$  ion in case of the KOH solution [31,32].

Apart from being more abundant and less expensive than PGM, silver exhibits good activity toward oxygen reduction [9]. Copper and cobalt are proven to enhance the physical and chemical properties of the catalyst upon addition, including the increase in the number of active sites, specific surface, and conductivity [10,17]. Andrade et al. [17] have shown that MOF-derived N-doped carbon with cobalt and copper (M-NC-CoCu) has fast ORR kinetics with an onset potential,  $E_{onset}$ , of 0.85 V, a half-wave potential,  $E_{1/2}$ , of 0.75 V, and a small Tafel slope ( $63 \text{ mV dec}^{-1}$ ) in KOH. Under the same experimental conditions, the values for Pt/C were an  $E_{onset}$  of 0.93 V, an  $E_{1/2}$  of 0.82 V, and a Tafel slope of  $70 \text{ mV dec}^{-1}$ .

It has been well-documented that bimetallic nanoparticle electrocatalysts containing a noble metal (e.g., Pt, Au, Ag) and a transition metal (e.g., Co, Cu) overcome the performance of the individual components for the ORR due to the improvement of the electronic properties [33,34]. For instance, Verma et al. [9] proved that the Ag-Cu bimetallic particle formation enhances the catalytic properties of the material, which can be explained by DFT calculations showing that Cu to Ag charge transfer results in the stronger material's interaction with oxygen. Yin et al. [35] demonstrated that a catalyst containing both Ag and Cu particles exhibits a seven-fold enhancement of ORR activity compared to nanoporous Ag (NP-Ag). The former catalyst had an  $E_{1/2}$  of ca. 0.82 V and a Tafel slope of 100 mV dec<sup>-1</sup>, whereas that of NP-Ag and Pt/C was 145 mV dec<sup>-1</sup> and 111 mV dec<sup>-1</sup>, respectively. The results were supported by presenting XRD and XPS data showing that the d-band center of Ag moves closer to the Fermi level owing to the alloying effect from Cu. These conclusions extrapolate to other transition metals, especially 3d elements with fairly good conductivity and oxygen absorption properties, including cobalt. Carbon-based materials not only exhibit good catalytic activity for both HPRR and ORR, but the implementation of rGO in the bimetallic material also increases the specific surface area, improves thermal stability and electrical and thermal conductivity of the material, and heightens carrier mobility and adsorptive properties [36,37]. Therefore, the proposed materials are expected to show excellent activity for ORR.

## 2. Materials and Methods

Hydrazine hydrate ( $N_2H_4 \cdot xH_2O$ , 78 wt.%), cobalt chloride ( $CoCl_2 \cdot 6H_2O$ , 97 wt.%), copper chloride ( $CuCl_2 \cdot 2H_2O$ , 97 wt.%), L-ascorbic acid ( $C_6H_8O_6$ , 99 wt.%), sodium borohydride ( $NaBH_4$ , 99 wt.%), silver nitrate ( $AgNO_3$ , 99 wt.%), potassium permanganate ( $KMnO_4$ , 99 wt.%), Nafion (5 wt.%), methanol ( $CH_3OH$ , 97 wt.%), ethanol ( $C_2H_5OH$ , 99.8 wt.%) sodium hydroxide ( $NaOH$ , 97 wt.%), and potassium hydroxide ( $KOH$ , 85 wt.%) were obtained from Sigma-Aldrich (Burlington, MA, USA). The aqueous solutions were prepared by using distilled water.

Graphene oxide (GO) was synthesized by a modified Hummer's method [38]. Namely, GO was prepared from graphite, where 2 g of graphite powder was dispersed in 100 mL concentrated  $H_2SO_4$ . This solution was cooled at 0 °C, and then 8 g of  $KMnO_4$  was gradually added with a constant stirring at 30 °C for 1 h. Next, 300 mL distilled water was added to the solution with a continuous stirring for 30 min at 90 °C. 400 mL distilled water and 6 mL  $H_2O_2$  (30 wt.%) were added to the solution, where the solution color changed from dark brown to yellow-green. The obtained GO was separated by centrifuging and dried at 80 °C.

Reduced graphene oxide (rGO) was obtained in the second synthesis phase with  $N_2H_4 \cdot xH_2O$  as a reducing agent. Namely, 100 mg GO and 100 mL distilled water were mixed. This brown-yellow solution was left in the ultrasound bath at 150 W until this solution stayed without visible particles. Then 1 mL of 32.1 M  $N_2H_4 \cdot xH_2O$  was added, and the solution was heated at 100 °C, under a condenser, for further 24 h. The rGO was then separated by filtration as a black precipitate. After filtration, the rGO was washed 5 times with 100 mL distilled water and 5 times with 100 mL  $CH_3OH$ , and then dried.

The procedure described by Krishna et al. [39] was followed with some changes. A total of 35 mg rGO was well dispersed in 11.6 mL distilled water, and then it was mixed with 167 mg  $CoCl_2 \cdot 6H_2O$  (or 172 mg  $CuCl_2 \cdot 2H_2O$ ) by magnetic stirring for 30 min at room temperature. Then, 117 mg of L-ascorbic acid was added to the above solution and stirred for 10 min. Additionally, 5 mL of 1 M  $NaBH_4$  + 0.1 M  $NaOH$  solution was slowly added (dropwise) until the hydrogen was completely released. The obtained product was washed with distilled water and  $CH_3OH$ , respectively.

This product was again redispersed in distilled water by sonication for 1 h. A total of 60 mg  $AgNO_3$  was mixed with obtained dispersion by mechanically stirring for 5 min. Then, 17 mg of L-ascorbic acid was added to the solution with 1 mL of 1 M  $NaBH_4$  +

0.1 M NaOH solution to reduce Ag ions. The CuAg/rGO and CoAg/rGO products were washed several times with distilled water and dried in the oven at 80 °C for 4 h.

Fourier transform infrared spectroscopy (FTIR, Perkin Elmer Spectrum One Spectrometer, Waltham, MA, USA) and Raman spectroscopy (Leica Microsystems GmbH, Wetzlar, Germany) were used to determine surface functional groups of the rGO, CuAg/rGO, and CoAg/rGO electrocatalysts. X-ray diffraction analysis (XRD) using a Rigaku Ultima IV diffractometer (Rigaku, Japan) in Bragg-Brentano geometry, with Ni-filtered CuK $\alpha$  radiation ( $\lambda = 1.54178 \text{ \AA}$ ) was used for examining the structure of CuAg/rGO and CoAg/rGO electrocatalysts. The morphology and microstructure of CuAg/rGO and CoAg/rGO electrocatalysts were examined by transmission electron microscopy (TEM) using a HITACHI H-8100 microscope (Hitachi, Tokyo, Japan). Scanning electron microscopy with integrated energy-dispersive X-ray spectroscopy (SEM-EDS) detector was done with a scanning electron microscope Phenom<sup>TM</sup> ProX Desktop SEM (ThermoFisher Scientific<sup>TM</sup>, Waltham, MA, USA) to examine the surface morphology and atomic composition of CoAg/rGO and CuAg/rGO electrocatalysts. Cu, Co, and Ag wt.% in the two samples were determined by inductively coupled plasma with optical emission spectroscopy (ICP-OES) using an ICP optical emission spectrometer Optima 7000DV (Perkin Elmer, Waltham, MA, USA).

A total of 5 mg of powdered CuAg/rGO or CoAg/rGO were mixed with 980  $\mu\text{L}$  of C<sub>2</sub>H<sub>5</sub>OH and 20  $\mu\text{L}$  of Nafion (5%) and left in an ultrasonic bath for 1 h. After that, 14  $\mu\text{L}$  of the prepared catalytic ink was pipetted onto a glassy carbon rotating disk electrode (RDE, 0.19625 cm<sup>2</sup>). The electrode was left to dry at room temperature.

Ivium VO1107 potentiostat/galvanostat (Ivium Technologies B.V., Eindhoven, The Netherlands) was used for all electrochemical studies in a three-electrode system. A saturated calomel electrode (SCE, HI5412, Hanna Instruments) and a graphite rod (Sigma-Aldrich, 99.995 wt.%) were employed as reference and counter electrodes, respectively. The supporting electrolyte was 0.1 M KOH. As the SCE can suffer from instability in highly alkaline media, the potential difference between the herein used SCE and unused SCE was regularly measured using a multimeter, to ensure the quality of SCE potential measurements. All potentials in this work were converted to the reversible hydrogen electrode (RHE) scale using the following equation:  $E_{\text{RHE}} = E_{\text{SCE}} + 0.242 \text{ V} + 0.059 \text{ V} \times \text{pH}$ . Current densities were calculated using the geometric area.

Cyclic voltammograms (CVs) of CuAg/rGO and CoAg/rGO electrodes were recorded from 0.86 to 0.96 V at different polarization rates ranging from 5 to 100 mV s<sup>-1</sup> in 0.1 M KOH solution saturated with nitrogen (N<sub>2</sub>, 99.995 vol.%, Messer).

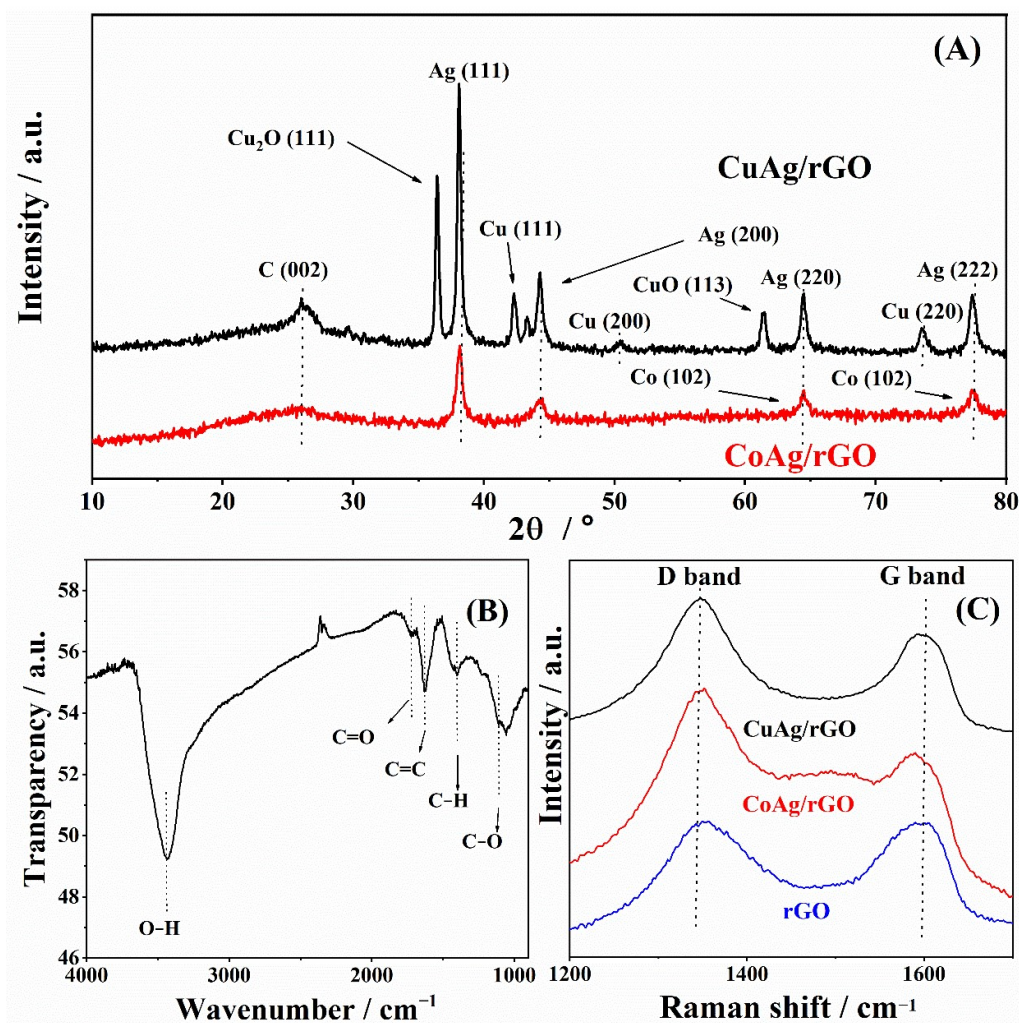
For ORR studies, linear sweep voltammograms (LSVs) were recorded in a potential range from 0.2 to 1 V at a scan rate of 20 mV s<sup>-1</sup> in 0.1 M KOH solution saturated with oxygen (O<sub>2</sub>, 99.995 vol.%, Messer) at room temperature. ORR rotating-disk electrode (RDE) measurements were carried out at different rotation rates from 400 to 3600 rpm. Current densities obtained in N<sub>2</sub>-saturated solutions were subtracted from those measured in O<sub>2</sub>-saturated solutions. Stability tests of CuAg/rGO and CoAg/rGO electrocatalysts were done in 0.1 M KOH O<sub>2</sub>-saturated solutions at 0.6 V for 4 h. HPRR LSVs were recorded in a potential range from 0.2 to 1 V at a scan rate of 20 mV s<sup>-1</sup> in 0.05 M H<sub>2</sub>O<sub>2</sub> + 0.1 M KOH solution saturated with N<sub>2</sub>.

### 3. Results and Discussion

#### 3.1. Characterization of CuAg/rGO and CoAg/rGO Electrocatalysts

The XRD analysis of CuAg/rGO and CoAg/rGO electrocatalysts is presented in Figure 1A. The peak at about 26° was observed at both XRD patterns of CuAg/rGO and CoAg/rGO electrodes as a reflection of the C (002) plane [40]. Four characteristic diffraction peaks of bulk metallic Ag at 2 $\theta$  of ca. 38.3°, 44.4°, 64.5°, and 77.5° were noticed for both electrodes as the diffraction from crystal planes of Ag (111), (200), (220), and (222), respectively [40–42]. The XRD pattern of the CuAg/rGO electrode showed a diffraction peak of the Cu<sub>2</sub>O(111) plane at ca. 36° and three diffraction peaks of Cu (111), (200), and (220) crystal planes at 2 $\theta$  of ca. 42.3°, 50.4°, and 73.6°, respectively [43]. Two diffraction

peaks of Co appeared at  $2\theta$  of ca.  $64.5$  and  $77.5^\circ$ , corresponding to the reflections of the Co (102) and (103) planes, respectively [44].

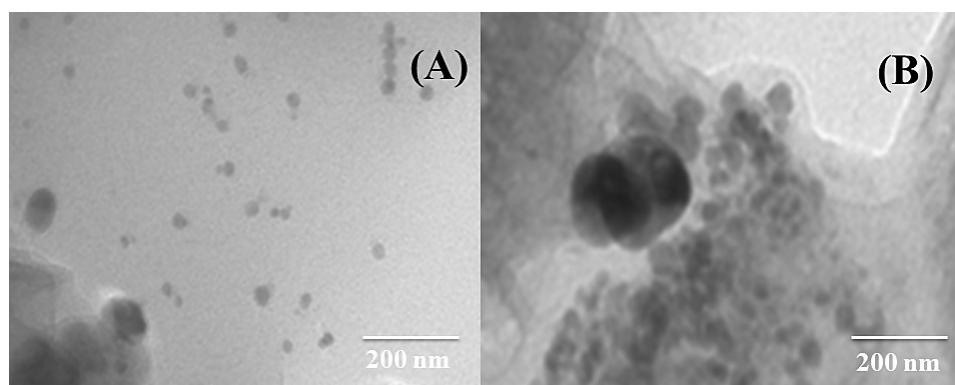


**Figure 1.** XRD patterns of CuAg/rGO and CoAg/rGO electrocatalysts (A). FTIR of rGO (B) and Raman spectra of rGO, CuAg/rGO, and CoAg/rGO electrocatalysts (C).

The FTIR spectrum of rGO is presented in Figure 1B, where a broad peak was noticed at  $3438\text{ cm}^{-1}$ , corresponding to the  $\text{OH}^-$  groups of water adsorbed on rGO [45,46]. The adsorption peaks at  $1724$ ,  $1623$ , and  $1103\text{ cm}^{-1}$  were visible for the characteristic carboxyl group C=O, an aromatic C=C group, and a C-O group, respectively [45,46].

The Raman spectra of rGO, CuAg/rGO, and CoAg/rGO (Figure 1C) show two characteristic strong peaks, known as D and G bands, at  $1351$  and  $1595\text{ cm}^{-1}$  for rGO, at  $1346$  and  $1591\text{ cm}^{-1}$  for CuAg/rGO, and at  $1350$  and  $1596\text{ cm}^{-1}$  for CoAg/rGO [45]. The G band corresponds to the bond extending of all pairs of  $\text{sp}^2$  atoms, whereas the D band represents the presence of structural defects, crystal imperfections, and the measure of the degree of disorder of carbon-based materials [45,46]. The 2D called G' band characteristic for graphite materials was noticed at  $2704\text{ cm}^{-1}$  [45,47,48]. The D + G peak also related to disorder with structure was obtained at  $2933\text{ cm}^{-1}$  [45,47,48]. The intensity ratio of the D and G bands ( $I_D/I_G$ ) was found to be  $0.85$  for rGO, CuAg/rGO, and CoAg/rGO. The broad, low-intensity peak at about  $1483\text{ cm}^{-1}$  for CoAg/rGO could be related to the specific structure of  $\text{Ag}_2\text{O}$  [49]. These results utterly confirmed the presence of an rGO structure in CuAg/rGO and CoAg/rGO electrocatalysts.

Figure 2A,B shows TEM images of CuAg/rGO and CoAg/rGO electrocatalysts, revealing the formation of metal nanoparticles.



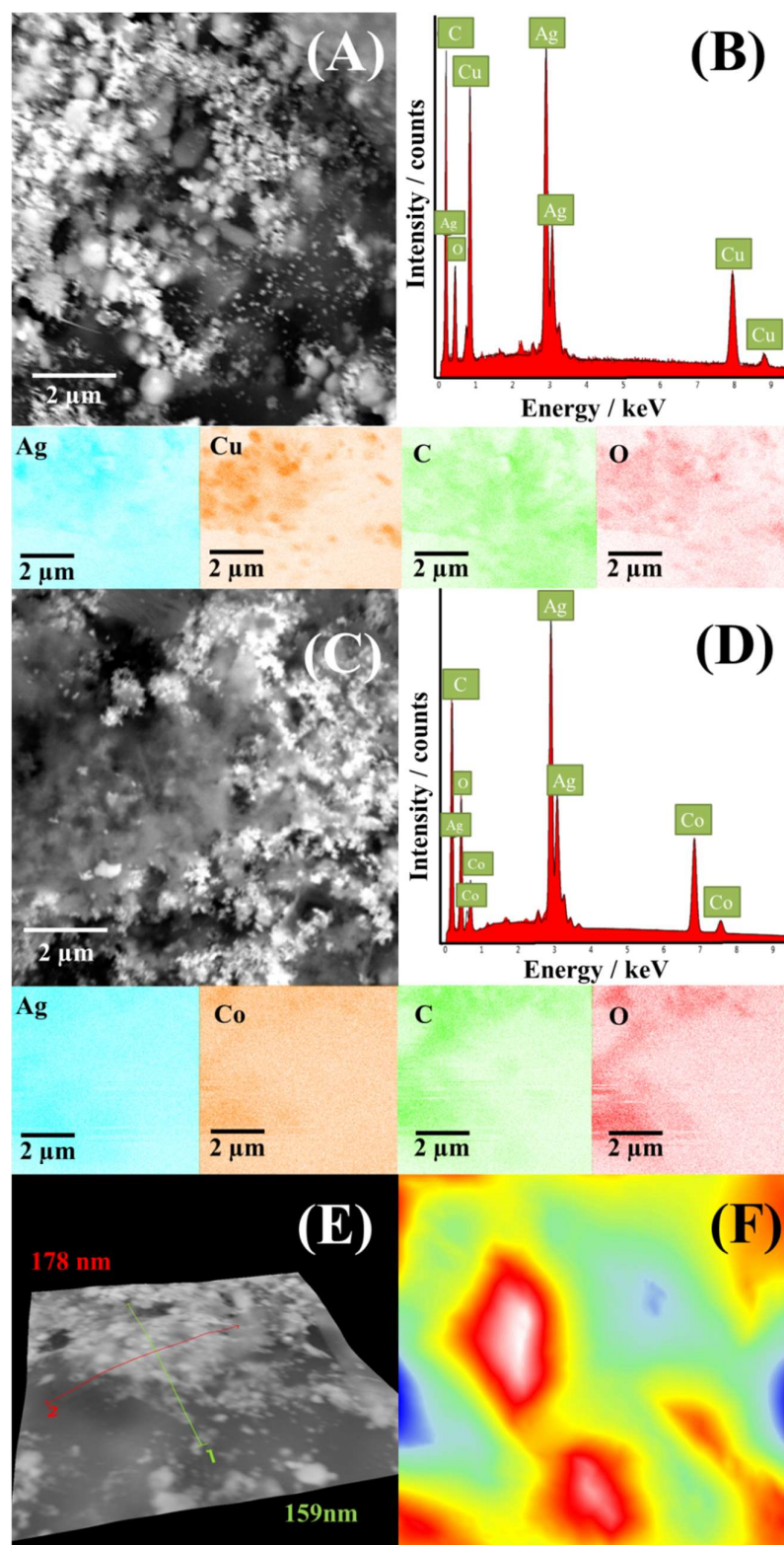
**Figure 2.** TEM images of CuAg/rGO (A) and CoAg/rGO (B) electrocatalysts.

SEM images of CuAg/rGO and CoAg/rGO electrocatalysts with corresponding EDS spectra and mapping are presented in Figure 3. SEM images of CuAg/rGO and CoAg/rGO (Figure 3A,C) show a uniform distribution of metal nanoparticles (bright parts) over rGO (gray parts). Corresponding EDS spectra and mapping (Figure 3B,D) show the presence of Ag, Cu, Co, C, and O elements and confirm their uniform distribution.

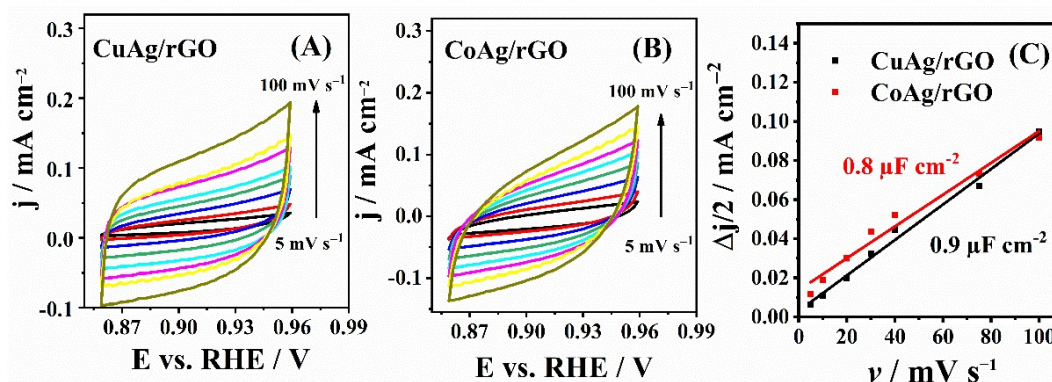
The elemental composition of the electrocatalysts determined by ICP-OES shows 27.8 and 31.5 wt.% of Ag and Cu, respectively, for CuAg/rGO and 27.0 and 17.3 wt.% of Ag and Co, respectively, for CoAg/rGO. Though the present study was “conceived” as an initial study to confirm or disprove AgCo and/or AgCu on rGO as electrocatalysts for the ORR and to point out the path that further research should take, it should be noted that the electrocatalytic performance of bimetallic nanoparticles is governed by their composition, among other factors, including particle size and surface oxidation state [33,50,51].

Electrochemical double-layer capacitance,  $C_{dl}$ , was calculated from cyclic voltammograms (CVs) of CuAg/rGO and CoAg/rGO electrocatalysts (Figure 4) recorded in  $N_2$ -saturated 0.1 M KOH solution at different scan rates.  $C_{dl}$  was found to be 0.9 and 0.8  $\mu F cm^{-2}$  for CuAg/rGO and CoAg/rGO, respectively, with these values being directly proportional to the electrochemically active surface area (ECSA) [52,53]. The somewhat higher ECSA of CuAg/rGO than CoAg/rGO electrocatalyst represents the higher number of active sites for ORR and HPRR [52,53]. It should be mentioned that high-surface-area rGO contributes to the non-faradaic, capacitive currents and, consequently, affects the accurate ECSA determination. Still, the present ECSA estimation by the  $C_{dl}$  method is suitable for the ECSAs comparison, as both materials contain rGO. Moreover, the  $C_{dl}$  method for estimating alloys' ECSA considers all the alloy components [54,55].

Regarding the nature of active sites in the two electrocatalysts, the Ag(111) plane has been pointed out as highly active toward ORR, where the presence of different defects further increases the surface's activity for ORR [56]. The higher availability of active sites for ORR on Ag(111) is attributed to the weaker  $OH^-$  adsorption. Furthermore, Co (moiety) has been presented as an important active site for ORR in alkaline media [57–60]. Cu shows high theoretical ORR activity in the volcano plot and has four valence states (Cu(I), Cu(II), Cu(0), and Cu(IV)) which contribute to ORR electrocatalysis [61]. Finally, the presence of rGO also brings different types of surface active sites for ORR, including unsaturated carbons defect sites and carbon-oxygen polar groups.



**Figure 3.** SEM images of CuAg/rGO (A) and CoAg/rGO (C) electrocatalysts with the corresponding EDS spectrum of CuAg/rGO (B) and CoAg/rGO (D) and mapping images of Ag, Cu, Co, C, and O with the corresponding 3D SEM surface reconstruction (E,F).



**Figure 4.** CVs of CuAg/rGO (A) and CoAg/rGO (B) electrocatalysts and the corresponding double-layer capacitance plots (C) in N<sub>2</sub>-saturated 0.1 M KOH solution at different scan rates.

### 3.2. ORR Activity of CuAg/rGO and CoAg/rGO Electrocatalysts

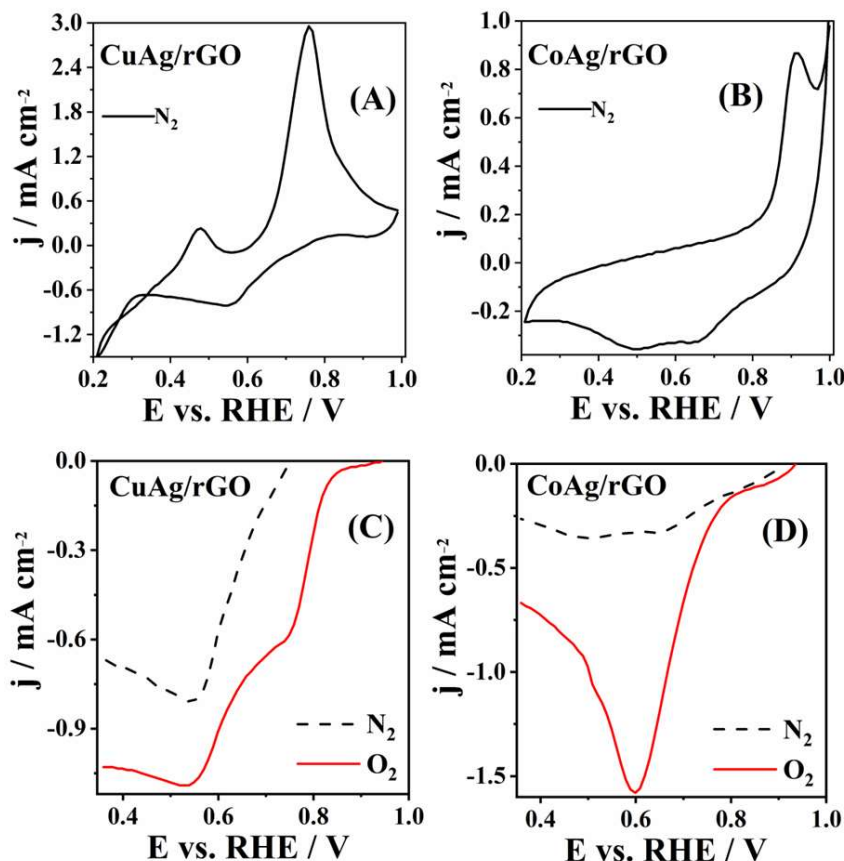
CVs of CuAg/rGO and CoAg/rGO electrocatalysts recorded in N<sub>2</sub>-saturated solution are presented in Figure 5A,B. Two well-defined anodic peaks appearing at 0.47 and 0.76 V (Figure 5A) are attributed to the oxidation of the CuAg/rGO surface, where the first anodic peak presents the oxidation of Cu(0) to Cu(I), and the second anodic peak presents the oxidation of Cu(I) to Cu(II) [62,63]. An additional cathodic peak was noticed at 0.55 V corresponding to the reduction of Cu(II) to Cu(I) [62,63]. The CoAg/rGO electrocatalyst showed one anodic peak at 0.92 V (Figure 5B) corresponding to the oxidation Co(II) to Co(III) [64,65]. Figure 5C,D presents ORR polarization curves of CuAg/rGO and CoAg/rGO electrocatalysts, where both materials show ORR activity in 0.1 M KOH. The CoAg/rGO electrocatalyst exhibited a current density of  $-1.56$  and  $-0.34$  mA cm<sup>-2</sup>, at 0.6 V, in O<sub>2</sub> and N<sub>2</sub>-saturated solution, respectively (Figure 5D). The current density of  $-0.58$  and  $-0.03$  mA cm<sup>-2</sup>, at 0.7 V, for the first cathodic peak and  $-1.1$  and  $-0.82$  mA cm<sup>-2</sup>, at 0.5 V, for the second cathodic peak were noticed for the CuAg/rGO electrocatalyst in O<sub>2</sub> and N<sub>2</sub>-saturated solution, respectively (Figure 5C). CuAg/rGO and CoAg/rGO gave about 20 (first reduction peak) and 5 times higher cathodic current densities, respectively, in O<sub>2</sub>-saturated than in deaerated solution (Figure 5C,D). Even 50% times higher ORR current was observed for CoAg/rGO than for the CuAg/rGO electrocatalyst. An Ag/Co/C hybrid electrocatalyst was recently pointed out as a promising candidate for ORR in alkaline media because of its excellent ORR activity and stability [13]. This behavior of Ag/Co/C during ORR was described by density functional theory (DFT), where ORR starts due to the strong interaction between Co and O in the first step, and the following steps on the Ag surface occur with a small barrier [13]. Additionally, Verma et al. showed that oxygen adsorption on Ag clusters increased by doping with copper atoms, confirmed by binding energy DFT calculations [9].

ORR polarization curves of CuAg/rGO and CoAg/rGO electrocatalysts obtained at 1600 rpm in O<sub>2</sub>-saturated solution are presented in Figure 6A.  $E_{\text{onset}}$  and  $E_{1/2}$  were found to be 0.81 and 0.71 V for CuAg/rGO and 0.76 and 0.62 V for CoAg/rGO, respectively. Thus, CuAg/rGO showed 50 and 90 mV more positive ORR  $E_{\text{onset}}$  and  $E_{1/2}$ , respectively, compared to the CoAg/rGO electrocatalyst. Ag@CuO nanoparticles showed  $E_{1/2}$  of 0.74 V [66], which is ca. 30 mV more positive than the herein examined CuAg/rGO electrocatalyst.

The ORR kinetics was examined by Tafel analysis of the curves presented in Figure 6A. Tafel slopes of 184 and 109 mV dec<sup>-1</sup> for CuAg/rGO and CoAg/rGO were calculated. The CoAg/rGO electrocatalyst showed a lower Tafel slope than CuAg/rGO, indicating faster ORR kinetics. The big difference in Tafel slopes can be a consequence of differences in the physicochemical properties of the CuAg/rGO and CoAg/rGO surface, such as oxygen coverage and the number of active sites [56]. Nanoporous Ag (NP-Ag) [35] and monometallic Ag nanoparticles (Ag NPs) [67] showed a Tafel slope of 145 and 113 mV dec<sup>-1</sup> during ORR in 0.1 M KOH, respectively. A Tafel slope of 96 mV dec<sup>-1</sup> was determined



for Ag/OCPN at the low current density region [68]. S. Zoladec et al., determined Tafel slopes of 100 and 120  $\text{mV dec}^{-1}$  for silver nanoparticles deposited on rGO-carboxylate and rGO-SiO<sub>2</sub>, respectively [56]. Five different nanoporous AgCu (NP-AgCu) catalysts gave Tafel slopes ranging from 100 to 124  $\text{mV dec}^{-1}$  in 0.1 M KOH [35]. CuO nanoparticles (CuO) and CuO nanoparticles on graphene (CuO/G) showed a Tafel slope of 207 and 141  $\text{mV dec}^{-1}$ , respectively [69].

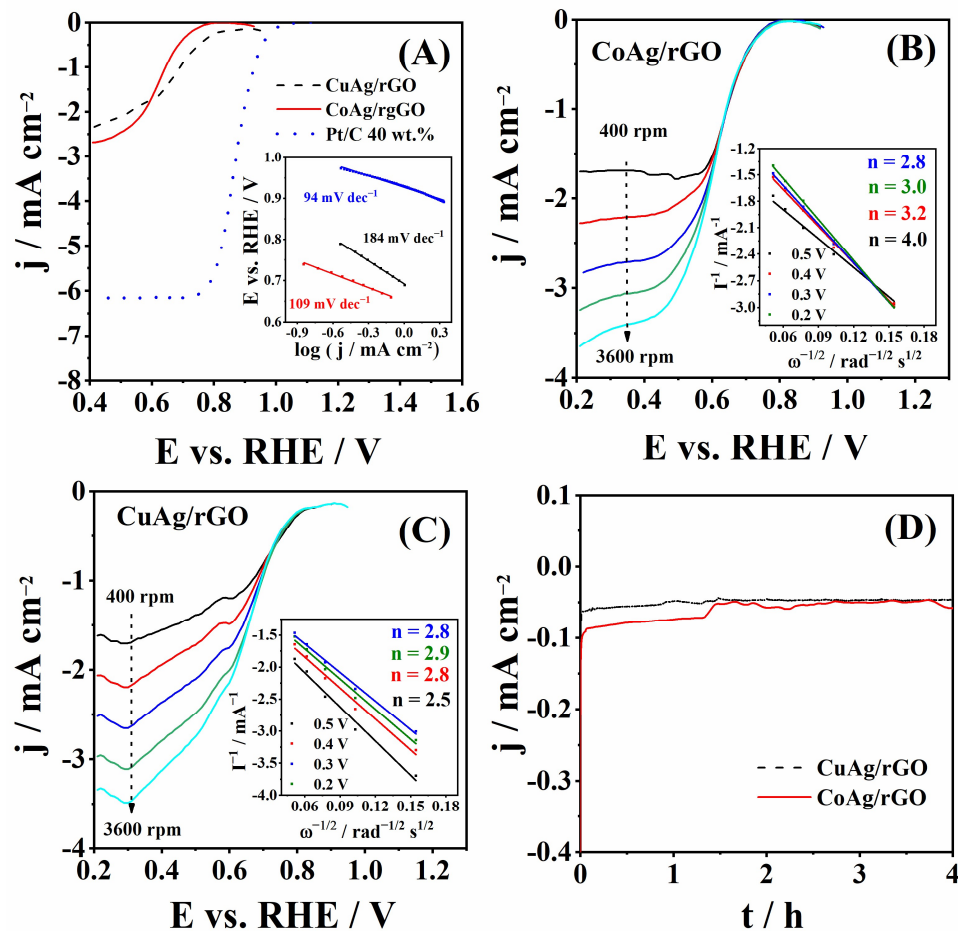


**Figure 5.** CVs of CuAg/rGO (A) and CoAg/rGO (B) electrocatalysts recorded at 20  $\text{mV s}^{-1}$  in N<sub>2</sub>-saturated 0.1 M KOH solution and the cathodic part of CVs of CuAg/rGO (C) and CoAg/rGO (D) electrocatalysts recorded at 20  $\text{mV s}^{-1}$  in N<sub>2</sub>- and O<sub>2</sub>-saturated 0.1 M KOH solution.

Furthermore, a higher diffusion current density,  $j_d$ , was obtained for CoAg/rGO ( $-2.63 \text{ mA cm}^{-2}$ ) than for the CuAg/rGO ( $-1.74 \text{ mA cm}^{-2}$ ) electrocatalyst. Ag/C gave a  $j_d$  of ca.  $-1.8 \text{ mA cm}^{-2}$  than herein tested silver electrocatalysts in alkaline media [70]. A  $j_d$  of  $-2.8 \text{ mA cm}^{-2}$  was obtained for Ag/Co<sub>3</sub>O<sub>4</sub>-C composite in 1 M KOH, comparable with the  $j_d$  obtained for CoAg/rGO [70]. ORR performance of two prepared electrocatalysts was further compared to that of commercial Pt/C (40 wt.% Pt), Figure 6A. As expected, higher current densities were recorded with the Pt/C electrode, along with a Tafel slope of 94  $\text{mV dec}^{-1}$ . However, the significantly lower price of the herein prepared electrocatalysts and the possibility of further improvement of their performance justify their use for ORR studies.

Figure 6B,C shows the ORR polarization curves of CoAg/rGO and CuAg/rGO electrocatalysts, respectively, at different rotation rates, ranging from 400 to 3600 rpm. From these data, Koutecky-Levich analysis calculated the number of exchanged electrons,  $n$ , during ORR in alkaline media [41]. The value of  $n$  was found to range from 2.8 to 4.0 and from 2.5 to 2.9 for CoAg/rGO and CuAg/rGO electrocatalysts (inset of Figure 6B,C), respectively, suggesting that ORR occurred by the mixed  $2e^-$  and  $4e^-$  reduction pathway. [70,71]. It is worth noting that at a more positive potential, four electrons were transferred during

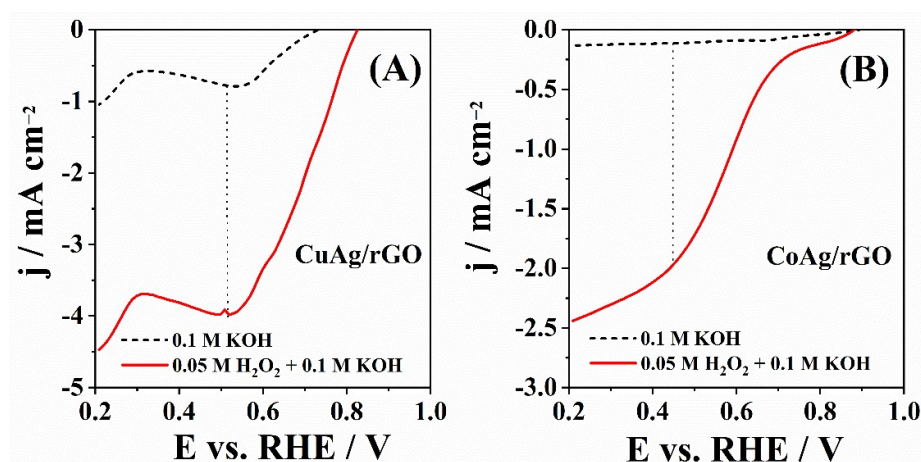
ORR at CoAg/rGO. The transfer of four electrons during ORR at Ag-based electrocatalysts often involves a  $2e^- + 2e^-$  series mechanism rather than a direct  $4e^-$  mechanism. Thus, the HPRR activity of the prepared electrocatalysts was also probed.



**Figure 6.** ORR polarization curves measured at  $20 \text{ mV s}^{-1}$  and 1600 rpm with the corresponding Tafel plots shown in the inset (A), ORR polarization curves of CoAg/rGO (B) and CuAg/rGO (C) electrocatalysts at different rotation rates with Koutecky-Levich analysis in the inset, and the chronoamperometric curves (D) recorded in  $\text{O}_2$ -saturated 0.1 M KOH solution.

Figure 7 shows LSVs of CuAg/rGO and CoAg/rGO electrocatalysts recorded in 0.1 M KOH solution as a supporting electrolyte in the absence and presence of  $\text{H}_2\text{O}_2$ . Both materials showed electrocatalytic activity for HPRR with a reduction peak at ca. 0.50 and 0.45 V for CuAg/rGO and CoAg/rGO electrocatalysts, respectively. Carbon paste electrodes modified by Ag-supported carbon microspheres (Ag-CMS/CPE) obtained by the hydrothermal method showed a similar HPRR peak potential value in alkaline media [72]. CuAg/rGO showed a higher peak current density of  $-3.96 \text{ mA cm}^{-2}$  than CoAg/rGO electrocatalyst ( $-1.96 \text{ mA cm}^{-2}$ ).

It should be mentioned that the ORR at the currently examined CoAg/rGO electrocatalyst led to a higher  $n$  than at Ag/C, with 2.7 electrons exchanged during ORR in alkaline media [70]. Ag@C nano cables delivered 3.3 electrons during ORR in 0.1 M KOH [71]. Silver and copper nanocatalysts supported with multi-walled carbon nanotube (AgCu/MWCNT) delivered 3.5 electrons during ORR in alkaline media [73]. Table 1 compares the ORR parameters determined for CuAg/rGO and CoAg/rGO electrocatalysts with that previously reported for similar materials.



**Figure 7.** LSVs of CuAg/rGO (A) and CoAg/rGO (B) electrocatalysts recorded at  $20 \text{ mV s}^{-1}$  in  $\text{N}_2$ -saturated  $0.1 \text{ M KOH}$  solution without (–) and with (–)  $0.05 \text{ M H}_2\text{O}_2$ .

**Table 1.** Comparison of ORR parameters of CuAg/rGO and CoAg/rGO electrocatalysts with the activity of similar materials reported in the literature.

ORR Catalysts	$j_d@(\text{1600 rpm})$ $/\text{mA cm}^{-2}$	$E_{\text{onset}}/\text{V}$	$E_{1/2}/\text{V}$	$n$	Source
CuAg/rGO	−1.74	0.81	0.71	2.5–2.9	This work
CoAg/rGO	−2.63	0.76	0.62	2.8–4.0	This work
$\text{Ag}_9\text{Cu}_1/\text{MWCNT}^*$	−2.7	–	–	3.5	[73]
Ag/C	−1.8	–	–	2.7	[70]
Co/C	−2.48	0.88	0.83	–	[13]
Ag@CuO	–	–	0.74	3.8	[66]
Ag@C nanocables	−2.5	0.75	–	3.3	[71]
Ag/Co <sub>3</sub> O <sub>4</sub> -C	−2.8	0.84	0.78	3.8	[70]
Ag/CPN**	−4.8	0.83	–	3.7	[68]
Ag/OCPN***	−5.4	0.87	–	4.0	[68]

\* MWCNT—multi-walled carbon nanotubes, \*\* CPN—carbonaceous polypyrrole nanotubes, \*\*\* OCPN—oxygen-doped carbonaceous polypyrrole nanotubes.

To confirm the stability of the electrocatalysts' activity towards ORR in alkaline media, chronoamperometric curves of CuAg/rGO and CoAg/rGO electrocatalysts were run for 4 h (Figure 6D). Both electrocatalysts showed good stability for ORR. Current densities of  $-0.046$  and  $-0.055 \text{ mA cm}^{-2}$  were obtained for CuAg/rGO and CoAg/rGO at 4 h, representing ca. 28 and 29% decrease of the corresponding initial values. For both electrocatalysts, the decrease was observed within the first 200 s, with fairly constant current densities for the rest of the measurement. Thus, the authors believe this decrease is caused by the adsorption of impurities on the surface of the electrocatalysts rather than by the metal nanoparticles' agglomeration or detachment [34].

#### 4. Conclusions

Silver copper and silver cobalt nanoparticles were deposited on synthesized rGO (CuAg/rGO and CoAg/rGO) and tested for ORR in alkaline media. Raman spectroscopy clearly showed that rGO was obtained during synthesis, and the surface morphology and atomic composition of CuAg/rGO and CoAg/rGO electrocatalysts were confirmed by SEM-EDS analysis. The average particle diameter obtained by TEM analysis for CuAg/rGO and CoAg/rGO electrocatalysts was 5.7 and 5.5 nm, respectively. CoAg/rGO showed a lower Tafel slope than the CuAg/rGO electrocatalyst. The lower Tafel slope, higher ORR current densities,  $j_d$ , and  $n$  of CoAg/rGO demonstrate faster ORR kinetics and better ORR catalytic activity than the CuAg/rGO electrocatalyst. Additionally, both electrocatalysts showed reasonable activity for HPRR, with a reduction peak at ca. 0.50 and 0.45 V for CuAg/rGO and CoAg/rGO, respectively. These electrocatalysts can potentially replace

high-cost platinum group metal-based catalysts because of their easy, fast, and low-cost synthesis, coupled with their good ORR activity and stability in alkaline media.

**Author Contributions:** Conceptualization, J.M., D.M.F.S. and B.Š.; Formal analysis, J.M., S.K., S.S. and F.A.H.; Funding acquisition, M.A., D.M.F.S. and B.Š.; Investigation, J.M., S.K. and S.S.; Project administration, D.M.F.S. and M.A.; Supervision, D.M.F.S. and B.Š.; Validation, F.A.H., M.A. and B.Š.; Visualization, J.M., D.M.F.S. and B.Š.; Writing—original draft, J.M. and S.K.; Writing—review & editing, D.M.F.S. and B.Š. All authors have read and agreed to the published version of the manuscript.

**Funding:** The authors would like to acknowledge the support of the Ministry of Education, Kingdom of Saudi Arabia for this research through a grant (PCSED-022-18) under the Promising Centre for Sensors and Electronic Devices (PCSED) at Najran University, Kingdom of Saudi Arabia. They also thank the Ministry of Education, Science and Technological Development of the Republic of Serbia for contract no. 451-03-68/2022-14/200146). Fundação para a Ciência e a Tecnologia (FCT, Portugal) is acknowledged for funding a research contract in the scope of programmatic funding UIDP/04540/2020 (D.M.F.S.) and contract no. IST-ID/156-2018 (B.Š.).

**Data Availability Statement:** Data available on request to the corresponding author.

**Acknowledgments:** The authors would like to thank Nemanja Gavrilov and Danica Bajuk-Bogdanović, University of Belgrade, Faculty of Physical Chemistry, for SEM/EDS and Raman spectroscopy analysis, respectively, as well as to Dalibor Stanković, University of Belgrade, Faculty of Chemistry, for ICP-OES analysis of the prepared samples.

**Conflicts of Interest:** The authors declare no conflict of interest. The funders had no role in the design of the study; in the collection, analyses, or interpretation of data; in the writing of the manuscript, or in the decision to publish the results.

## References

1. Rizo, R.; Feliu, J.M.; Herrero, E. New insights into the hydrogen peroxide reduction reaction and its comparison with the oxygen reduction reaction in alkaline media on well-defined platinum surfaces. *J. Catal.* **2021**, *398*, 123–132. [[CrossRef](#)]
2. Šljukić, B.; Santos, D.M.F. Chapter 10—Direct borohydride fuel cells (DBFCs). In *Direct Liquid Fuel Cells; Fundamentals, Advances and Future*; Akay, R.G., Yurtcan, A.B., Eds.; Academic Press: Cambridge, MS, USA, 2021; pp. 203–232. ISBN 978-0-12-818624-4.
3. Martos, V.B. Unraveling the Oxygen Reduction Reaction Mechanism: Occurrence of a Bifurcation Point before Hydrogen Peroxide Formation. Ph.D. Thesis, Universidad de Alicante, Alicante, Spain, 2019.
4. Ma, R.; Lin, G.; Zhou, Y.; Liu, Q.; Zhang, T.; Shan, G.; Yang, M.; Wang, J. A review of oxygen reduction mechanisms for metal-free carbon-based electrocatalysts. *NPJ Comput. Mater.* **2019**, *5*, 78. [[CrossRef](#)]
5. Daniel, G.; Zhang, Y.; Lanzalaco, S.; Brombin, F.; Kosmala, T.; Granozzi, G.; Wang, A.; Brillas, E.; Sirés, I.; Durante, C. Chitosan-Derived Nitrogen-Doped Carbon Electrocatalyst for a Sustainable Upgrade of Oxygen Reduction to Hydrogen Peroxide in UV-Assisted Electro-Fenton Water Treatment. *ACS Sustain. Chem. Eng.* **2020**, *8*, 14425–14440. [[CrossRef](#)]
6. Singh, D.K.; Ganesan, V.; Yadav, D.K.; Yadav, M.; Sonkar, P.K.; Gupta, R. Mesoporous carbon nitride supported 5,10,15,20-tetrakis(4-methoxyphenyl)-21H,23H-porphine cobalt(II) as a selective and durable electrocatalyst for the production of hydrogen peroxide via two-electron oxygen reduction. *Catal. Sci. Technol.* **2021**, *11*, 1014–1026. [[CrossRef](#)]
7. Deng, Z.; Ma, C.; Yan, S.; Dong, K.; Liu, Q.; Luo, Y.; Liu, Y.; Du, J.; Sun, X.; Zheng, B. One-dimensional conductive metal-organic framework nanorods: A highly selective electrocatalyst for the oxygen reduction to hydrogen peroxide. *J. Mater. Chem. A* **2021**, *9*, 20345–20349. [[CrossRef](#)]
8. Jeong, W.; Yin, C.L.; Hui, K.S.; Hui, K.N.; Cho, Y.R.; Cho, K.M. Enhanced electrochemical reduction of hydrogen peroxide by Co<sub>3</sub>O<sub>4</sub> nanowire electrode. *J. Mater. Sci. Mater. Electron.* **2017**, *28*, 16672–16678. [[CrossRef](#)]
9. Verma, A.; Gupta, R.K.; Shukla, M.; Malviya, M.; Sinha, I. Ag–Cu Bimetallic Nanoparticles as Efficient Oxygen Reduction Reaction Electrocatalysts in Alkaline Media. *J. Nanosci. Nanotechnol.* **2019**, *20*, 1765–1772. [[CrossRef](#)]
10. Wang, H.; Wei, L.; Liu, J.; Shen, J. Hollow bimetal ZIFs derived Cu/Co/N co-coordinated ORR electrocatalyst for microbial fuel cells. *Int. J. Hydrogen Energy* **2020**, *45*, 4481–4489. [[CrossRef](#)]
11. Li, H.; Yin, J.; Meng, Y.; Liu, S.; Jiao, T. Nickel/Cobalt-Containing polypyrrole hydrogel-derived approach for efficient ORR electrocatalyst. *Colloids Surf. A Physicochem. Eng. Asp.* **2020**, *586*, 124221. [[CrossRef](#)]
12. Liu, A.; Li, C.; Ren, X.; Gao, L.; Ma, T. Co loaded on graphene with interfacial structure as high performance catalyst for 4e<sup>−</sup> ORR: A DFT study. *Ionics* **2020**, *26*, 3483–3490. [[CrossRef](#)]
13. Qiu, Y.; Hu, Z.; Li, H.; Ren, Q.; Chen, Y.; Hu, S. Hybrid electrocatalyst Ag/Co/C via flash Joule heating for oxygen reduction reaction in alkaline media. *Chem. Eng. J.* **2022**, *430*, 132769. [[CrossRef](#)]

14. Gong, L.; Li, X.; Zhang, Q.; Huang, B.; Yang, Q.; Yang, G.; Liu, Y. Ultrafast and large-scale synthesis of Co<sub>3</sub>O<sub>4</sub> quantum dots-C<sub>3</sub>N<sub>4</sub>/rGO as an excellent ORR electrocatalyst via a controllable deflagration strategy. *Appl. Surf. Sci.* **2020**, *525*, 146624. [[CrossRef](#)]
15. Wang, Y.; Gan, R.; Ai, Z.; Liu, H.; Wei, C.; Song, Y.; Dirican, M.; Zhang, X.; Ma, C.; Shi, J. Hollow Co<sub>3</sub>O<sub>4-x</sub> nanoparticles decorated N-doped porous carbon prepared by one-step pyrolysis as an efficient ORR electrocatalyst for rechargeable Zn-air batteries. *Carbon* **2021**, *181*, 87–98. [[CrossRef](#)]
16. Wang, Y.; Gan, R.; Liu, H.; Dirican, M.; Wei, C.; Ma, C.; Shi, J.; Zhang, X. Fe<sub>3</sub>O<sub>4</sub>/Fe<sub>2</sub>O<sub>3</sub>/Fe nanoparticles anchored on N-doped hierarchically porous carbon nanospheres as a high-efficiency ORR electrocatalyst for rechargeable Zn-air batteries. *J. Mater. Chem. A* **2021**, *9*, 2764–2774. [[CrossRef](#)]
17. Macedo Andrade, A.; Liu, Z.; Grewal, S.; Nelson, A.J.; Nasef, Z.; Diaz, G.; Lee, M.H. MOF-derived Co/Cu-embedded N-doped carbon for trifunctional ORR/OER/HER catalysis in alkaline media. *Dalton Trans.* **2021**, *50*, 5473–5482. [[CrossRef](#)]
18. Li, Y.W.; Zhang, W.J.; Li, J.; Ma, H.Y.; Du, H.M.; Li, D.C.; Wang, S.N.; Zhao, J.S.; Dou, J.M.; Xu, L. Fe-MOF-Derived Efficient ORR/OER Bifunctional Electrocatalyst for Rechargeable Zinc-Air Batteries. *ACS Appl. Mater. Interfaces* **2020**, *12*, 44710–44719. [[CrossRef](#)] [[PubMed](#)]
19. Yu, H.; Hou, J.; Namin, R.B.; Ni, Y.; Liu, S.; Yu, S.; Liu, Y.; Wu, Q.; Nie, S. Pre-cryocrushing of natural carbon precursors to prepare nitrogen, sulfur co-doped porous microcellular carbon as an efficient ORR catalyst. *Carbon* **2021**, *173*, 800–808. [[CrossRef](#)]
20. Huang, N.B.; Zhang, J.J.; Sun, Y.; Sun, X.N.; Qiu, Z.Y.; Ge, X.W. A non-traditional biomass-derived N, P, and S ternary self-doped 3D multichannel carbon ORR electrocatalyst. *New J. Chem.* **2020**, *44*, 14604–14614. [[CrossRef](#)]
21. Radwan, A.; Jin, H.; Liu, B.; Chen, Z.; Wu, Q.; Zhao, X.; He, D.; Mu, S. 3D-ZIF scaffold derived carbon encapsulated iron nitride as a synergistic catalyst for ORR and zinc-air battery cathodes. *Carbon* **2021**, *171*, 368–375. [[CrossRef](#)]
22. Hamam, A.; Dehchar, C.; Maiza, M.; Chikouche, I.; Merabti, H. Facile synthesis and electrochemical study of CuO thin films for hydrogen peroxide reduction in alkaline medium. *Int. J. Electrochem. Sci.* **2020**, *15*, 3534–3542. [[CrossRef](#)]
23. Gutierrez, F.A.; Mazario, E.; Menéndez, N.; Herrasti, P.; Rubianes, M.D.; Zagal, J.H.; Yañez, C.; Rivas, G.A.; Bollo, S.; Recio, F.J. Electrocatalytic Activity of Nanohybrids Based on Carbon Nanomaterials and MFe<sub>2</sub>O<sub>4</sub> (M=Co, Mn) towards the Reduction of Hydrogen Peroxide. *Electroanalysis* **2018**, *30*, 1613–1618. [[CrossRef](#)]
24. Rodrigues, W.V.; Nascimento, S.Q.; Silva, W.Y.S.; Quinzeiro, S.F.L.; Luz, R.A.S.; Cantanhêde, W. Structural reorganization of CuO/Cu<sub>2</sub>[Fe(CN)<sub>6</sub>] nanocomposite: Characterization and electrocatalytic effect for the hydrogen peroxide reduction. *An. Acad. Bras. Cienc.* **2020**, *92*, e20191442. [[CrossRef](#)]
25. Brzózka, A.; Brudzisz, A.; Jeleń, A.; Kozak, M.; Wesół, J.; Iwaniec, M.; Sulka, G.D. A comparative study of electrocatalytic reduction of hydrogen peroxide at carbon rod electrodes decorated with silver particles. *Mater. Sci. Eng. B Solid-State Mater. Adv. Technol.* **2021**, *263*, 114801. [[CrossRef](#)]
26. Hsu, S.Y.; Lee, C.L.; Kuo, C.H.; Kuo, W.C. Defective graphene nanosheets with heteroatom doping as hydrogen peroxide reduction catalysts and sensors. *Sens. Actuators B Chem.* **2021**, *328*, 129015. [[CrossRef](#)]
27. Wang, T.P.; Lee, C.L.; Kuo, C.H.; Kuo, W.C. Potential-induced sonoelectrochemical graphene nanosheets with vacancies as hydrogen peroxide reduction catalysts and sensors. *Ultrason. Sonochem.* **2021**, *72*, 105444. [[CrossRef](#)]
28. Chen, Z.; Li, G.; Liu, Y.; Shi, P.; Li, F. Novel Co<sub>1-x</sub>S/C-3 supported on N-doped ketjen black as an efficient electrocatalyst for oxygen reduction reaction in alkaline media. *J. Taiwan Inst. Chem. Eng.* **2020**, *106*, 215–226. [[CrossRef](#)]
29. Sandhiran, N.; Ganapathy, S.; Manoharan, Y.; Ganguly, D.; Kumar, M.; Ramanujam, K.; Balachandran, S. CuO–NiO binary transition metal oxide nanoparticle anchored on rGO nanosheets as high-performance electrocatalyst for the oxygen reduction reaction. *Environ. Res.* **2022**, *211*, 112992. [[CrossRef](#)] [[PubMed](#)]
30. Spendelov, J.S.; Wieckowski, A. Electrocatalysis of oxygen reduction and small alcohol oxidation in alkaline media. *Phys. Chem. Chem. Phys.* **2007**, *9*, 2654–2675. [[CrossRef](#)]
31. Elezovic, N.R.; Babic, B.M.; Radmilovic, V.R.; Vracar, L.M.; Krstajic, N.V. Nb-TiO<sub>2</sub> supported platinum nanocatalyst for oxygen reduction reaction in alkaline solutions. *Electrochim. Acta* **2011**, *56*, 9020–9026. [[CrossRef](#)]
32. Hsueh, K.L.; Gonzalez, E.R.; Srinivasan, S. Electrolyte effects on oxygen reduction kinetics at platinum: A rotating ring-disc electrode analysis. *Electrochim. Acta* **1983**, *28*, 691–697. [[CrossRef](#)]
33. Bakir, A.C.; Şahin, N.; Polat, R.; Dursun, Z. Electrocatalytic reduction of oxygen on bimetallic copper-gold nanoparticles-multiwalled carbon nanotube modified glassy carbon electrode in alkaline solution. *J. Electroanal. Chem.* **2011**, *662*, 275–280. [[CrossRef](#)]
34. Alekseeva, E.; Stelmashuk, T.; Danilov, S.; Yang, P.; Levin, O. Bimetallic Cu/Pt oxygen reduction reaction catalyst for fuel cells cathode materials. *Catalysts* **2020**, *10*, 667. [[CrossRef](#)]
35. Yin, S.; Shen, Y.; Zhang, J.; Yin, H.M.; Liu, X.Z.; Ding, Y. Tuning the electronic structure of nanoporous Ag via alloying effect from Cu to boost the ORR and Zn-air battery performance. *Appl. Surf. Sci.* **2021**, *545*, 149042. [[CrossRef](#)]
36. Singh, H.; Zhuang, S.; Ingis, B.; Nunna, B.B.; Lee, E.S. Carbon-based catalysts for oxygen reduction reaction: A review on degradation mechanisms. *Carbon* **2019**, *151*, 160–174. [[CrossRef](#)]
37. Yu, H.; Guo, W.; Lu, X.; Xu, H.; Yang, Q.; Tan, J.; Zhang, W. Reduced graphene oxide nanocomposite based electrochemical biosensors for monitoring foodborne pathogenic bacteria: A review. *Food Control* **2021**, *127*, 108117. [[CrossRef](#)]

38. Sun, L.; Wang, L.; Tian, C.; Tan, T.; Xie, Y.; Shi, K.; Li, M.; Fu, H. Nitrogen-doped graphene with high nitrogen level via a one-step hydrothermal reaction of graphene oxide with urea for superior capacitive energy storage. *RSC Adv.* **2012**, *2*, 4498–4506. [[CrossRef](#)]
39. Krishna, R.; Fernandes, D.M.; Dias, C.; Ventura, J.; Venkata Ramana, E.; Freire, C.; Titus, E. Novel synthesis of Ag@Co/RGO nanocomposite and its high catalytic activity towards hydrogenation of 4-nitrophenol to 4-aminophenol. *Int. J. Hydrogen Energy* **2015**, *40*, 4996–5005. [[CrossRef](#)]
40. Xu, X.; Tan, C.; Liu, H.; Wang, F.; Li, Z.; Liu, J.; Ji, J. Carbon black supported ultra-high loading silver nanoparticle catalyst and its enhanced electrocatalytic activity towards oxygen reduction reaction in alkaline medium. *J. Electroanal. Chem.* **2013**, *696*, 9–14. [[CrossRef](#)]
41. Stoševski, I.; Krstić, J.; Milikić, J.; Šljukić, B.; Kačarević-Popović, Z.; Mentus, S.; Miljanić, Š. Radiolotically synthesized nano Ag/C catalysts for oxygen reduction and borohydride oxidation reactions in alkaline media, for potential applications in fuel cells. *Energy* **2016**, *101*, 79–90. [[CrossRef](#)]
42. Gan, T.; Lv, Z.; Sun, J.; Shi, Z.; Liu, Y. Preparation of graphene oxide-wrapped carbon sphere@silver spheres for high performance chlorinated phenols sensor. *J. Hazard. Mater.* **2016**, *302*, 188–197. [[CrossRef](#)]
43. Shokry Hassan, H.; Kashyout, A.B.; Morsi, I.; Nasser, A.A.A.; Abuklill, H. Development of polypyrrole coated copper nanowires for gas sensor application. *Sens. Bio-Sens. Res.* **2015**, *5*, 50–54. [[CrossRef](#)]
44. Saha, S.; Ganguly, S.; Banerjee, D.; Kargupta, K. Novel bimetallic graphene-cobalt-nickel (G-Co-Ni) nano-ensemble electrocatalyst for enhanced borohydride oxidation. *Int. J. Hydrogen Energy* **2015**, *40*, 1760–1773. [[CrossRef](#)]
45. Alam, S.N.; Sharma, N.; Kumar, L. Synthesis of Graphene Oxide (GO) by Modified Hummers Method and Its Thermal Reduction to Obtain Reduced Graphene Oxide (rGO)\*. *Graphene* **2017**, *6*, 1–18. [[CrossRef](#)]
46. Chanda, D.; Hná, J.R.; Dobrota, A.S.; Paš, I.A.; Paidar, M.; Bouzek, K. The effect of surface modification by reduced graphene oxide on the electrocatalytic activity of nickel towards the hydrogen evolution reaction. *Phys. Chem. Chem. Phys.* **2015**, *17*, 26864–26874. [[CrossRef](#)] [[PubMed](#)]
47. Marinoiu, A.; Raceanu, M.; Andrulevicius, M.; Tamuleviciene, A.; Tamulevicius, T.; Nica, S.; Bala, D.; Varlam, M. Low-cost preparation method of well dispersed gold nanoparticles on reduced graphene oxide and electrocatalytic stability in PEM fuel cell. *Arab. J. Chem.* **2020**, *13*, 3585–3600. [[CrossRef](#)]
48. Zoladek, S.; Rutkowska, I.A.; Blicharska, M.; Miecznikowski, K.; Ozimek, W.; Orłowska, J.; Negro, E.; Di Noto, V.; Kulesza, P.J. Evaluation of reduced-graphene-oxide-supported gold nanoparticles as catalytic system for electroreduction of oxygen in alkaline electrolyte. *Electrochim. Acta* **2017**, *233*, 113–122. [[CrossRef](#)]
49. Yang, Z.; Zhang, L.; You, H.; Li, Z.; Fang, J. Particle-arrayed silver mesocubes synthesized via reducing silver oxide mesocrystals for surface-enhanced raman spectroscopy. *Part. Part. Syst. Character.* **2014**, *31*, 390–397. [[CrossRef](#)]
50. Linge, J.M.; Erikson, H.; Merisalu, M.; Sammelselg, V.; Tammeveski, K. Oxygen reduction on silver catalysts electrodeposited on various nanocarbon supports. *SN Appl. Sci.* **2021**, *3*, 263. [[CrossRef](#)]
51. Lu, A.; Peng, D.L.; Chang, F.; Skeete, Z.; Shan, S.; Sharma, A.; Luo, J.; Zhong, C.J. Composition- and Structure-Tunable Gold-Cobalt Nanoparticles and Electrocatalytic Synergy for Oxygen Evolution Reaction. *ACS Appl. Mater. Interfaces* **2016**, *8*, 20082–20091. [[CrossRef](#)]
52. Ma, T.Y.; Dai, S.; Jaroniec, M.; Qiao, S.Z. Metal-organic framework derived hybrid Co<sub>3</sub>O<sub>4</sub>-carbon porous nanowire arrays as reversible oxygen evolution electrodes. *J. Am. Chem. Soc.* **2014**, *136*, 13925–13931. [[CrossRef](#)]
53. Gao, T.; Jin, Z.; Liao, M.; Xiao, J.; Yuan, H.; Xiao, D. A trimetallic V-Co-Fe oxide nanoparticle as an efficient and stable electrocatalyst for oxygen evolution reaction. *J. Mater. Chem. A* **2015**, *3*, 17763–17770. [[CrossRef](#)]
54. Lukaszewski, M.; Soszko, M.; Czerwiński, A. Electrochemical methods of real surface area determination of noble metal electrodes—An overview. *Int. J. Electrochem. Sci.* **2016**, *11*, 4442–4469. [[CrossRef](#)]
55. Radinović, K.; Mladenovic, D.; Milikić, J.; Alsaiani, M.; Harraz, F.A.; Santos, D.M.F.; Šljukić, B. Tuning Electrocatalytic Activity of Gold Silver Nanoparticles on Reduced Graphene Oxide for Oxygen Reduction Reaction. *J. Electrochem. Soc.* **2022**, *169*, 54501. [[CrossRef](#)]
56. Zoladek, S.; Blicharska-Sobolewska, M.; Krata, A.A.; Rutkowska, I.A.; Wadas, A.; Miecznikowski, K.; Negro, E.; Vezzù, K.; Di Noto, V.; Kulesza, P.J. Heteropolytungstate-assisted fabrication and deposition of catalytic silver nanoparticles on different reduced graphene oxide supports: Electroreduction of oxygen in alkaline electrolyte. *J. Electroanal. Chem.* **2020**, *875*, 114694. [[CrossRef](#)]
57. Zhang, A.; Wu, J.; Xue, L.; Yan, S.; Zeng, S. Probing Heteroatomic Dopant-Activity Synergy over Co<sub>3</sub>O<sub>4</sub>/Doped Carbon Nanotube Electrocatalysts for Oxygen Reduction Reaction. *Inorg. Chem.* **2020**, *59*, 403–414. [[CrossRef](#)] [[PubMed](#)]
58. Zheng, B.; Wang, J.; Wang, F.B.; Xia, X.H. Low-loading cobalt coupled with nitrogen-doped porous graphene as excellent electrocatalyst for oxygen reduction reaction. *J. Mater. Chem. A* **2014**, *2*, 9079–9084. [[CrossRef](#)]
59. Zdolšek, N.; Vujković, M.; Metin, Ö.; Brković, S.; Jocić, A.; Dimitrijević, A.; Trtić-Petrović, T.; Šljukić, B. Boosting electrocatalysis of oxygen reduction and evolution reactions with cost-effective cobalt and nitrogen-doped carbons prepared by simple carbonization of ionic liquids. *Int. J. Hydrogen Energy* **2022**, *47*, 14847–14858. [[CrossRef](#)]
60. Zhong, H.; Campos-Roldán, C.A.; Zhao, Y.; Zhang, S.; Feng, Y.; Alonso-Vante, N. Recent advances of cobalt-based electrocatalysts for oxygen electrode reactions and hydrogen evolution reaction. *Catalysts* **2018**, *8*, 559. [[CrossRef](#)]

61. Chen, X.L.; Zhu, H.B.; Ding, L.F. Cu dopant triggering remarkable enhancement in activity and durability of Fe-N-C electrocatalysts toward oxygen reduction. *J. Electroanal. Chem.* **2020**, *873*, 114389. [[CrossRef](#)]
62. Teo, W.Z.; Ambrosi, A.; Pumera, M. Direct electrochemistry of copper oxide nanoparticles in alkaline media. *Electrochem. Commun.* **2013**, *28*, 51–53. [[CrossRef](#)]
63. Bhowmick, S.; Alam, S.; Shah, A.K.; Qureshi, M. Bimetallic cyclic redox couple in dimanganese copper oxide supported by nickel borate for boosted alkaline electrocatalytic oxygen evolution reaction. *Sustain. Energy Fuels* **2021**, *5*, 2517–2527. [[CrossRef](#)]
64. Flores, C.L.I.; Balela, M.D.L. Electrocatalytic oxygen evolution reaction of hierarchical micro/nanostructured mixed transition cobalt oxide in alkaline medium. *J. Solid State Electrochem.* **2020**, *24*, 891–904. [[CrossRef](#)]
65. Huang, D.; Luo, Y.; Li, S.; Zhang, B.; Shen, Y.; Wang, M. Active catalysts based on cobalt oxide@cobalt/N-C nanocomposites for oxygen reduction reaction in alkaline solutions. *Nano Res.* **2014**, *7*, 1054–1064. [[CrossRef](#)]
66. Im, H.; Noh, S.; Shim, J.H. Spontaneous formation of core-shell silver-copper oxide by carbon dot-mediated reduction for enhanced oxygen electrocatalysis. *Electrochim. Acta* **2020**, *329*, 135172. [[CrossRef](#)]
67. Balkan, T.; Küçükkeçeci, H.; Zarenezhad, H.; Kaya, S.; Metin, Ö. One-pot synthesis of monodisperse copper–silver alloy nanoparticles and their composition-dependent electrocatalytic activity for oxygen reduction reaction. *J. Alloys Compd.* **2020**, *831*, 154787. [[CrossRef](#)]
68. Xiao, D.; Ma, J.; Chen, C.; Luo, Q.; Ma, J.; Zheng, L.; Zuo, X. Oxygen-doped carbonaceous polypyrrole nanotubes-supported Ag nanoparticle as electrocatalyst for oxygen reduction reaction in alkaline solution. *Mater. Res. Bull.* **2018**, *105*, 184–191. [[CrossRef](#)]
69. Yu, J.; Huang, T.; Jiang, Z.; Sun, M.; Tang, C. A hybrid material combined copper oxide with graphene for an oxygen reduction reaction in an alkaline medium. *Molecules* **2019**, *24*, 441. [[CrossRef](#)]
70. Wang, Y.; Lu, X.; Liu, Y.; Deng, Y. Silver supported on Co<sub>3</sub>O<sub>4</sub> modified carbon as electrocatalyst for oxygen reduction reaction in alkaline media. *Electrochem. Commun.* **2013**, *31*, 108–111. [[CrossRef](#)]
71. Chen, C.; Suryanto, B.H.R.; Zhao, C.; Jiang, X.; Yu, A. Direct Hydrothermal Synthesis of Carbonaceous Silver Nanocables for Electrocatalytic Applications. *Small* **2015**, *11*, 3557–3567. [[CrossRef](#)]
72. Randjelović, M.S.; Momčilović, M.Z.; Enke, D.; Mirčeski, V. Electrochemistry of hydrogen peroxide reduction reaction on carbon paste electrodes modified by Ag- and Pt-supported carbon microspheres. *J. Solid State Electrochem.* **2019**, *23*, 1257–1267. [[CrossRef](#)]
73. Yi, Q.; Chu, H.; Tang, M.; Yang, Z.; Chen, Q.; Liu, X. Carbon nanotube-supported binary silver-based nanocatalysts for oxygen reduction reaction in alkaline media. *J. Electroanal. Chem.* **2015**, *739*, 178–186. [[CrossRef](#)]